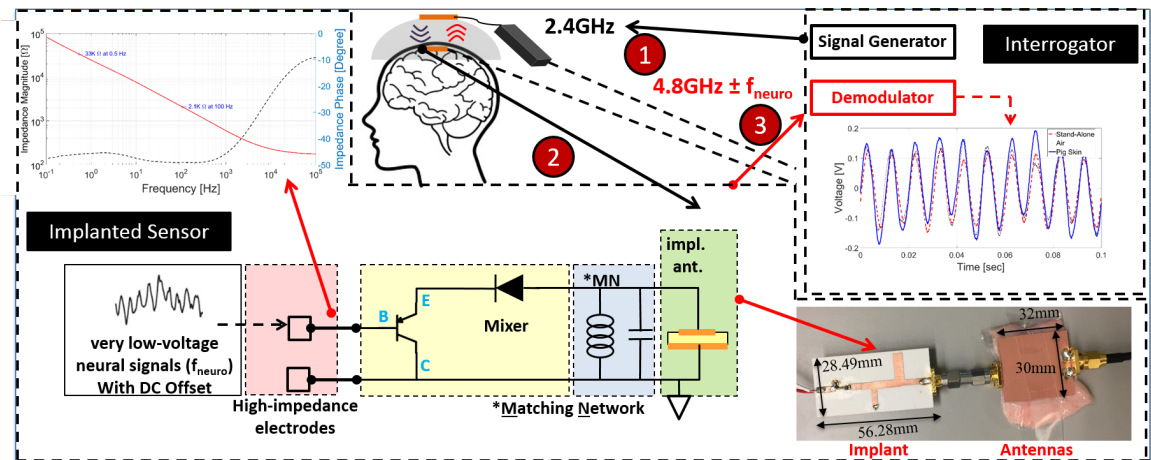


# Passive Impedance Matching For Implanted Brain-Electrode Interfaces

Wei-Chuan Chen, Student Member, IEEE, Katrina Guido, and Asimina Kiourti, Member, IEEE



Batteryless and wireless brain implants matched to high-impedance clinical electrodes.

- Radio-Frequency backscattering is employed to enable batteryless and wireless brain implants that are: a) matched to high-impedance clinical electrodes, and b) tolerant to DC voltage.
- As compared to previous wireless and batteryless brain implants, the proposed approach offers a remarkable improvement in sensitivity by 25 times.
- Unobtrusive monitoring of deep brain signals may significantly improve the individual's physical and mental well-being (e.g., for patients with epilepsy, Alzheimer's, Parkinson's, and more).
- Batteryless brain implants matched to high-impedance electrodes can readily be employed to clinical applications.
- Improvements on the interrogator side help suppress the phase noise and improve the demodulated signal integrity.

# Passive Impedance Matching For Implanted Brain-Electrode Interfaces

Wei-Chuan Chen, *Student Member, IEEE*, Katrina Guido, and Asimina Kiourti, *Member, IEEE*

**Abstract**—We propose a new technique for matching the high impedance of sub-cranial electrodes to wireless brain implants that is: a) passive, b) highly tolerant to the DC offset voltage caused by the electrochemical reaction in the recording electrode, and c) complemented by an improved external interrogator design that exhibits reduced phase noise. As compared to previous wireless and batteryless brain implants, the proposed approach offers a remarkable improvement in sensitivity by 25 times. The proposed system consists of an external interrogator and a neuro-recorder implanted under the scalp. For operation, the interrogator sends a 2.4 GHz carrier signal to “turn on” the implant. This carrier self-biases a PNP Bipolar Junction Transistor (BJT) that enables matching to the recording electrode at frequency  $f_{neuro}$  in a batteryless manner. Concurrently, the recorded neuropotentials (at frequency  $f_{neuro}$ ) pass through a Schottky diode that allows them to mix with the carrier and generate a  $4.8 \text{ GHz} \pm f_{neuro}$  modulated signal. The latter is then transmitted back to the interrogator for demodulation. To verify the implant's operation, *in-vitro* measurements are presented. Measurement results demonstrate that emulated neuropotentials as low as  $200 \mu\text{V}_{pp}$  can be detected at a  $33 \text{ k}\Omega$  electrode impedance. As such, the proposed system presents a game-changing capability for a wide range of applications.

**Keywords**—Biomedical telemetry, brain implant, DC offset, electrode, impedance matching, neurosensing, passive, wireless.

## I. INTRODUCTION

**R**ADIO-FREQUENCY (RF) backscattering is widely used today for applications as diverse as passive radio frequency identification (RFID), the Internet of Things (IoT), and so on. One emerging application of RF backscattering relates to wireless and fully-passive monitoring of deep brain activity [1]–[6]. Possible clinical applications include: 1) detection and interruption of early epileptic seizures, 2) behavioral studies of consciousness, 3) understanding and improving the brain's functionality for patients with Alzheimer's and Parkinson's disease [7], [8]. In brief, an external (wearable) interrogator sends a carrier signal toward an underlying batteryless implant. As soon as the implant turns on, it mixes the carrier with the sensed neuropotentials, and further backscatters the resulting mixing products back to the interrogator. Contrary to state-of-the-art integrated circuit (IC) brain implants, the aforementioned approach does not require implantable pre-amplifiers, digital controllers, Analog-to-Digital Converters (ADC), or other power-hungry components [9]–[11], thus eliminating batteries and temperature increase in the surrounding tissue [12].

Our latest research has demonstrated a miniature (8.7 mm x 10 mm) wireless and fully-passive brain implant with a remarkable  $20 \mu\text{V}_{pp}$  sensitivity under *in-vitro* conditions [3]. Such high sensitivity theoretically covers all signals generated by the human brain, including neural spikes and local field potentials (LFPs) [10]. Nevertheless, the aforementioned brain implant was optimized with *in-vitro* considerations in mind. That is, the implant was designed to match the impedance of a

TABLE I  
VOLTAGE AND FREQUENCY RANGE OF SIGNALS GENERATED BY THE HUMAN BRAIN [10]

Neural Signals	Voltage Range	Frequency Range
Local Field Potential	$20 \sim 2000 \mu\text{V}_{pp}$	$1 \sim 500 \text{ Hz}$
Action Potential	$20 \sim 2000 \mu\text{V}_{pp}$	$250 \text{ Hz} \sim 10 \text{ kHz}$
Electroencephalogram	$2 \sim 100 \mu\text{V}_{pp}$	$0.5 \text{ Hz} \sim 50 \text{ Hz}$

$50 \Omega$  function generator that emulated neuropotential activity. But unfortunately, the impedance of clinical electrodes is in the order of tens of  $\text{k}\Omega$ , implying a significant deterioration in sensitivity under *in-vivo* conditions. As an example, the sensitivity of the brain implant reported in [3] degrades from  $20 \mu\text{V}_{pp}$  to  $5 \text{ mV}_{pp}$  when attached to a  $33 \text{ k}\Omega$  resistor. Additionally, the DC offset voltage caused by the electrochemical reaction in the recording electrode is unaccounted for in [3]. Assuming an *in-vivo* scenario, this DC offset greatly changes the bias of the implanted diode used for mixing, further decreasing the system sensitivity.

Conventional integrated chips (ICs) used for neural recording utilize a first-stage neural amplifier that serves to increase the input impedance and cancel the DC offset voltage [13]. However, these neural amplifiers are typically associated with high power consumption and require very stable DC voltage supplies. Expectedly, integration of amplifiers is not a viable solution for our class of passive brain implants.

As an alternative, we herewith report a novel method for passively matching the high impedance of clinical electrodes to batteryless brain implants. To do so, a Bipolar Junction Transistor (BJT) is integrated into the implant and the overall circuit is redesigned accordingly. In brief, the BJT is self-biased by the external carrier and serves as an impedance buffer between the electrode and the circuitry. Concurrently, the DC offset voltage issue is eliminated. Modifications on the interrogator side of the circuit are also proposed to reduce

This paper is expanded from a presentation at the 2018 IEEE International Symposium on Antennas and Propagation and USNC-URSI Radio Science Meeting held in Boston, MA, USA.

W. Chen, K. Guido, and A. Kiourti are with the ElectroScience Laboratory, Department of Electrical and Computer Engineering, The Ohio State University, Columbus, OH 43212 USA (e-mail: chen.5825@osu.edu; guido.26@osu.edu; kiourti.1@osu.edu;)

This work was supported by the National Science Foundation under Grant 1763350.

the phase noise and further improve the integrity of the retrieved neuropotentials. To validate the above, an *in-vitro* measurement setup is considered with a series resistor used to account for the clinical electrode impedance.

## II. METHODS AND PROCEDURES

The block diagram of the proposed neurosensing system with impedance-matching capabilities is shown in Fig. 1. The system consists of two parts: 1) a brain implant placed under the scalp and attached to a recording electrode that penetrates through the bone to the cortical cortex surface, and 2) an external interrogator placed outside the scalp to communicate with the implanted sensor. Operation of the proposed system is summarized as follows. First, the external interrogator transmits a 2.4 GHz carrier signal via the interrogator antenna to activate the brain implant. This signal is rectified at the implanted diode and serves to self-bias the BJT. In turn, the high impedance of the BJT assists in matching to the high impedance of the recording electrode. Concurrently, the implanted diode acts as a mixer that uses the 2.4 GHz carrier to upconvert the brain signal (at frequency  $f_{neuro}$ ) to  $4.8 GHz \pm f_{neuro}$ . This upconverted third-order product is then backscattered by the implant's antenna and eventually received by the interrogator. This signal can then be directly observed in the frequency domain using a spectrum analyzer and/or can be demodulated and observed in the time domain using an oscilloscope.

To boost system sensitivity, a power budget analysis is hereafter presented. The ultimate aim is to lower the minimum detectable neuropotential level, expressed as:

$$MDS_{neuro}[dBm] = Receiver\ Sensitivity[dBm] + L_{sys}[dBm]. \quad (1)$$

where  $L_{sys}$  is the overall system loss, and *Receiver Sensitivity* is the minimum detectable signal level of the receiver (viz. the interrogator). Referring to Fig. 1, the overall system loss is expressed as:

$$L_{sys}[dB] = L_{prop}[dB] + L_{conv}[dB] + L_{circuit}[dB] + L_{electrode}[dB] \quad (2)$$

where  $L_{prop}$  is the propagation loss between the implanted and interrogator antenna at  $4.8 GHz \pm f_{neuro}$ ,  $L_{conv}$  is the conversion loss at the implanted mixer,  $L_{circuit}$  is the impedance mismatch loss between the antenna and the mixer, and  $L_{electrode}$  is the impedance mismatch loss between the recording electrode and the implant.

As is expected, to improve system sensitivity,  $L_{sys}$  must be minimized. Accordingly,  $L_{prop}$ ,  $L_{conv}$ ,  $L_{circuit}$  and  $L_{electrode}$  must be minimized to the greatest extent. Techniques for reducing  $L_{prop}$ ,  $L_{conv}$  and  $L_{circuit}$  were explored in our previous research [3]. Basically, low  $L_{prop}$  could be achieved by optimizing the implanted and interrogator antenna pair.  $L_{conv}$  and  $L_{circuit}$ , on the other hand, could be reduced by employing a matching network between the implanted antenna and the Schottky diode. In this work, we instead focus on reducing  $L_{electrode}$  by employing a new circuit design.

### A. Electrode Interface: Circuit Model and Impedance

When a clinical sub-cranial electrode is immersed inside a liquid-ionic conductor (electrolyte or buffer), the cations and anions react with the electrode and create an electrolyte-electrode double layer (namely, the Helmholtz double layer) [14]. The first layer of the Helmholtz double layer is composed of the ions absorbed on the surface by the charged electrodes. The second layer consists of the oppositely charged ions attracted by the Coulomb force. With these two oppositely charged layers, the metal electrode acts like a capacitor and allows the neuropotentials to pass through to the associated neural recorder [15].

The equivalent model of a sub-cranial electrode is well analyzed in the literature [16] and is illustrated in Fig. 2. As seen, the circuit model is composed of the electrolyte solution resistance ( $R_s$ ), the double layer interface resistance and capacitance ( $R_e$  and  $C_e$ ), and the metal electrode resistance ( $R_m$ ). Generally, the solution resistance ( $R_s$ ) and the metal electrode resistance ( $R_m$ ) are negligible as compared to the double layer interface resistance and capacitance ( $R_e$  and  $C_e$ ). Because of the double layer capacitance, the impedance of the electrode is a complex number and changes with frequency. Referring to Fig. 2, this electrode impedance degrades the signal amplitude at the input of the neuropotential monitoring system ( $V_{in}$ ) by means of a voltage divider:

$$V_{in}(\omega) = V_{sig}(\omega) \times \frac{Z_a}{Z_a + Z_e} \quad (3)$$

where  $V_{sig}$  is the neuropotential amplitude generated within the brain,  $Z_e$  is the complex electrode impedance, and  $Z_a$  is the complex neuro-sensor impedance. The voltage divider equation shows that the magnitude of  $Z_a$  would decrease  $V_{in}$  and cause phase distortion when  $Z_e \gg Z_a$  [16].

To better understand the effect of electrodes on the neurosensing system performance, we proceed to characterize via electrode impedance spectroscopy the impedance of clinical macro-electrodes currently used for Deep Brain Stimulation (DBS) surgery at Ohio State's Wexner Medical Center (FHC microTargeting mTD differential electrode) [17]. A potentiostat with a three-electrode setup is employed per Fig. 3. Here, the macroelectrode contact of the DBS electrode acts as the working electrode, while an Ag/AgCl and a Pt wire electrode are used as the reference and counter electrodes, respectively. All three electrodes are immersed inside a phosphate buffered saline (PBS) solution of pH 7.4 which mimics the pH, osmotic concentration, and ion concentration of the human body. Measurement results of electrode impedance magnitude and phase as a function of frequency are shown in Fig. 4. As seen, the impedance magnitude reduces with frequency. At the smallest frequency where neuropotentials may be identified, viz. at 0.5 Hz, the electrode impedance is as high as 33 k $\Omega$ .

Added to the above, the electrochemical reaction that takes place at the electrode interface will give rise to different DC voltage levels across different recording electrodes [18]–[20]. This voltage difference, which may be as high as 50 mV, known as the DC offset voltage, can have detrimental consequences. In conventional battery-enabled ICs, this offset is known to saturate the first-stage neural amplifier, while in

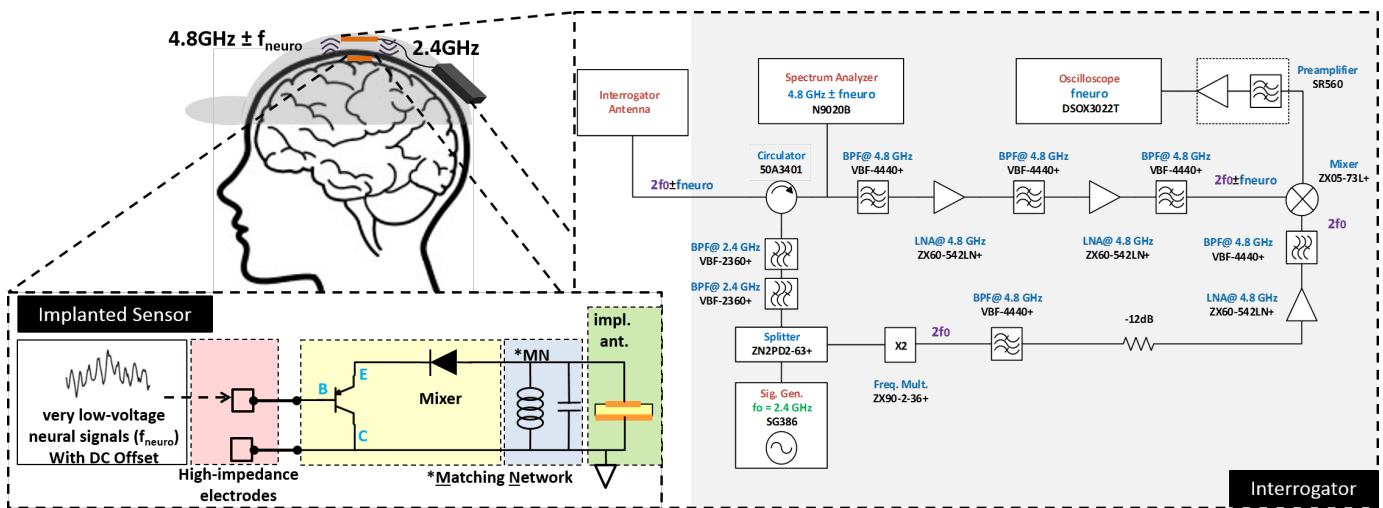


Fig. 1. Block diagram of the proposed impedance-matching neurosensing system.

our previous fully-passive neurosensing system [3], the offset is anticipated to change the bias point of the employed antiparallel diode pair (APDP) mixer and deteriorate the sensitivity.

These real-world concerns for clinical electrodes are hereafter taken into account. Given that neural signals may be as low as 0.5 Hz in frequency, a capability to match to at least 33 kΩ of electrode impedance is necessary for the neurosensing system of Fig. 1. Concurrently, the ability to overcome the DC offset voltage is a key requirement for the design.

### B. Passive Brain Implant with High Input Impedance

The operating principle of the proposed technique used to passively match the electrode-implant interface and eliminate the DC offset is summarized in Fig. 5. As seen, the implant consists of: a) an implantable antenna used for wireless backscattering, b) a Schottky diode that acts as a rectifier in DC mode and as a mixer in RF mode, c) a matching network used to mitigate  $L_{circuit}$  between the antenna and the Schottky diode (composed of two microstrip lines with open- and short-ended microstrip lines), d) the high-impedance clinical electrodes, and e) a PNP BJT added between the Schottky diode and the electrodes to serve as an impedance buffer.

Circuit operation is composed of two modes, viz. the DC mode (Fig. 5(a)) and the RF mode (Fig. 5(b)), as analyzed below.

1) DC Mode. To activate the neural sensor, the interrogator transmits a 2.4 GHz carrier signal. Once received by the

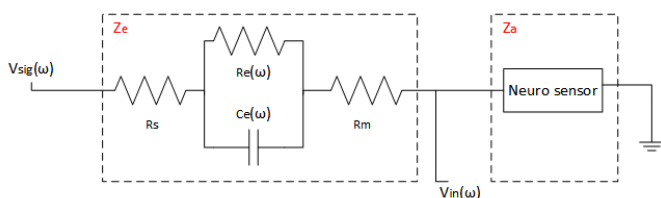


Fig. 2. Equivalent circuit model of the electrode.

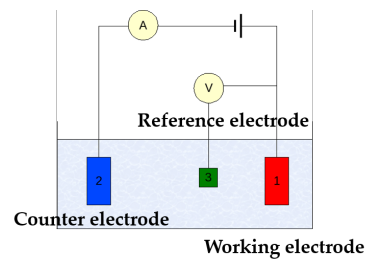


Fig. 3. Three electrode setup used to measure the electrode impedance using a potentiostat.

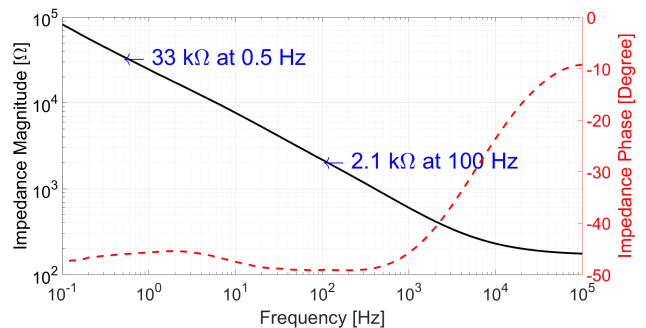


Fig. 4. Clinical brain electrode impedance measurement.

implant, the Schottky diode acts as a rectifier that serves to create DC current and self-bias the BJT per Fig. 5(a). Following biasing of the BJT, brain signals coming from its base should pass through the BJT and, eventually, get upconverted by the Schottky diode. To do so, the BJT emitter is connected right after the Schottky diode, while its collector is connected to ground. Comparing the voltages at the base ( $V_B$ ), collector ( $V_C$ ), and emitter ( $V_E$ ) terminals, the BJT may either operate in the forward-active region ( $V_E > V_B > V_C$ ) or the saturation region ( $V_E > V_B < V_C$ ), Table I. In both cases, signal may flow from the base to the emitter, while the DC voltage at the base may be neglected. This unique

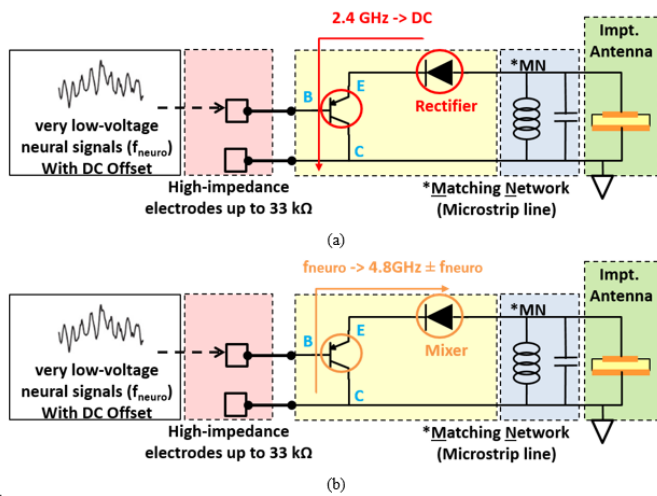


Fig. 5. Proposed neural implant design: (a) DC mode, and (b) RF mode.

TABLE II  
NODE VOLTAGE AND BJT OPERATION REGIONS

Voltage	B-E Junction	B-E Junction	Mode
$V_E < V_B < V_C$	Reverse	Forward	Reverse-active
$V_E < V_B > V_C$	Reverse	Reverse	Cut-off
$V_E > V_B < V_C$	Forward	Forward	Saturation
$V_E > V_B > V_C$	Forward	Reverse	Forward-active

feature implies tolerance to DC offset. Simulations indicate that the input impedance of the self-biasing BJT circuit is  $219\text{ k}\Omega$  and remains almost constant across the entire neural frequency range (0.5 Hz to 1 kHz). Due to the high input impedance of the BJT, the circuit of Fig. 5 can readily match to the high-impedance electrodes.

2) RF Mode. The Schottky diode now serves as a mixer, as shown in Fig. 5(b). That is, the diode utilizes the 2.4 GHz carrier signal to upconvert the brain signals (at frequency  $f_{neuro}$ ) and give rise to the third-order harmonic component ( $4.8\text{ GHz} \pm f_{neuro}$ ). This upconverted signal is backscattered toward the interrogator and is, eventually, demodulated to recover the neuropotentials in the time domain.

### C. Interrogator with Improved Phase Noise Performance

Instability of the signal generator that is used to generate the 2.4 GHz carrier creates phase noise. In the time domain and frequency domain, this noise appears as fluctuations and as a skirt centered at the carrier signal, respectively. While outputting the 2.4 GHz carrier, the signal generator also produces a 4.8 GHz harmonic which is, in turn, associated with its own phase noise. Unfortunately, this latter phase noise interferes with the demodulation process and has not been accounted for to date. To improve the interrogator's phase noise performance, the design in Fig. 1 is proposed. Compared to the previously employed interrogator system [3], two extra bandpass filters are added between the circulator and the splitter. Both filters are centered at 2.4 GHz and are used to suppress the 4.8

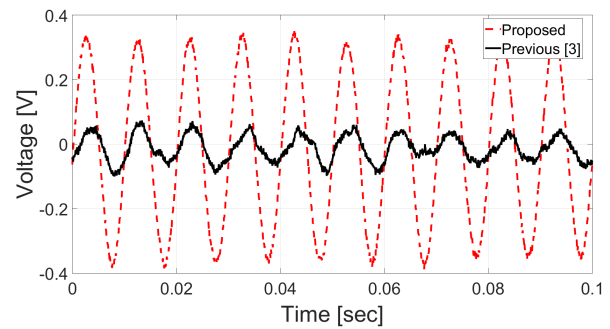


Fig. 6. Demodulated version of -115 dBm neural signal at 100 Hz. The plot compares the currently reported system vs. the one previously reported in [3].

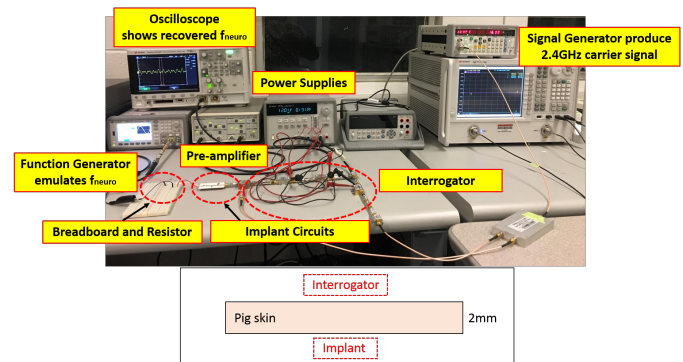


Fig. 7. Measurement set-up used to assess the neurosensing system performance.

GHz phase noise before it enters into the circulator. The superior performance of this interrogator is highlighted in Fig. 6. Here, a 100 Hz neural signal of -115 dBm is considered at the implant side, and the demodulated signal is contrasted at the output of the newly proposed interrogator vs. the one proposed in [3]. Clearly, the addition of the two bandpass filters significantly improves the retrieved signal integrity.

### D. Measurement Setup

The *in-vitro* measurement setup used to validate the neurosensing system of Fig. 1 is shown in Fig. 7. As depicted, a signal generator (Agilent SG386) feeds a 2.4 GHz carrier with 10 dBm signal level to the interrogator. An arbitrary function generator (Keysight 33500B) emulates neuropotentials as sinusoidal waveforms (at frequency  $f_{neuro}$ ). To consider a worst-case scenario for electrode impedance in this study, a  $33\text{ k}\Omega$  resistor is used to represent this impedance per Fig. 4. The improved interrogator of Fig. 1 demodulates the neuropotentials in the time domain. The demodulated neuropotentials are then visualized via an oscilloscope.

## III. RESULTS

### A. Stand-Alone Circuit Performance

As a first step, performance of the implanted circuit is tested in a stand-alone wired configuration. That is, the implanted antenna is not considered in the design, but rather the implanted circuit is directly connected to a circulator, as shown

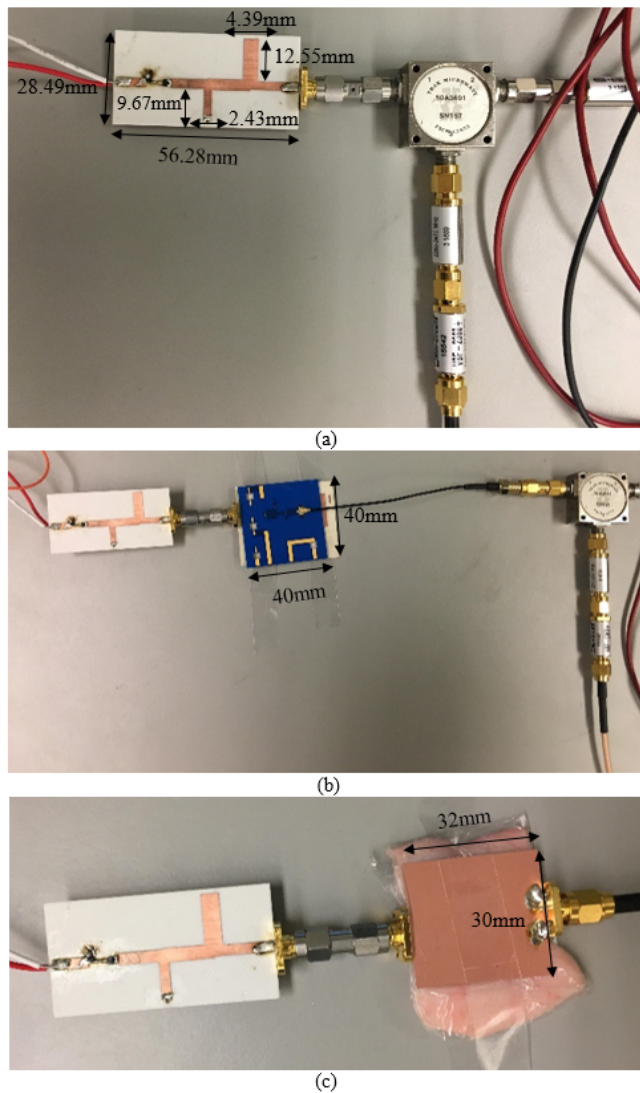


Fig. 8. Fabricated BJT Circuit (a) directly connected to circulator, (b) connected to antenna in air, and (c) connected to antenna in pig skin

in Fig. 8(a). Here, a proof-of-concept circuit, 56.28 mm  $\times$  28.49 mm in size, is considered. The circuit is fabricated on Rogers RO4003C substrate ( $\epsilon_r = 3.38$ ,  $\tan\delta = 0.0021$ ) of thickness 32 mils (0.813 mm). Miniaturization is outside the scope of this particular work, yet can be readily performed via techniques explored in the past [3]. Referring to Fig. 8(a), the 2.4 GHz carrier is set as the input to port 1 of the circulator and is routed directly to the implant through port 2. The implant mixes the carrier with the emulated neural signals and outputs the 4.8 GHz  $\pm f_{neuro}$  product to port 2 of the circulator. The latter signal is routed to port 3 of the circulator where it is, eventually, demodulated and plotted in the time domain.

Results show that neural signals as low as 100  $\mu V_{pp}$  can be retrieved for an electrode impedance of 33 k $\Omega$ . An example demodulated waveform at 100 Hz is shown in Fig. 9 (dashed/red), at the minimum detectable level of 100  $\mu V_{pp}$ . Expectedly, higher signal levels result in less noisy waveforms, while smaller electrode impedances result in improved sensitivity. For comparison, and assuming the same electrode

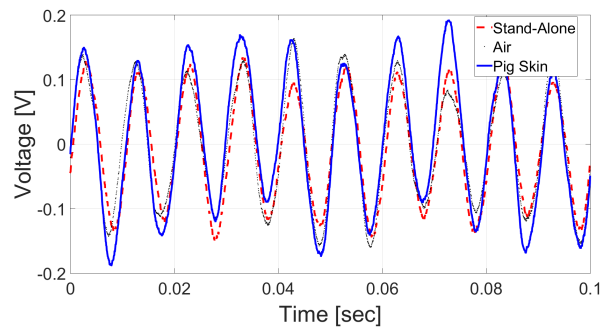


Fig. 9. The demodulated time domain 100 Hz signal of (a) circuit alone  $V_{in} = 100 \mu V_{pp}$ , (b) with the antenna in air  $V_{in} = 100 \mu V_{pp}$ , and (c) with the antenna in pig skin  $V_{in} = 200 \mu V_{pp}$  in series with a 33 k $\Omega$  resistor

impedance of 33 k $\Omega$ , the sensitivity of the neurosensing system in [3] is 50 times lower.

### B. Integrated System Performance

Performance of the complete wireless system is then validated in free space (Fig. 8(b)) and via a tissue-emulating model (Fig. 8(c)). In both cases, the implant circuit of Fig. 8(a) is attached to an antenna that serves as the wireless interface between the neuro-sensor and the interrogator. Here, the patch antenna design reported in [3] is considered, which exhibits dual-band resonances at 2.4/4.8 GHz and a footprint of 40 mm  $\times$  40 mm. Again, sensor miniaturization falls outside the scope of this work, yet can be readily performed using already available techniques [3]. The interrogator antenna follows the design in [4], while the overall system layout follows the design of Fig. 1.

Referring to Fig. 8(b), the implanted and interrogator antennas are placed in free-space with a distance of  $\sim 0.1$  m between the two. Results show that neural signals as low as 100  $\mu V_{pp}$  can be retrieved for an electrode impedance of 33 k $\Omega$ . An example demodulated waveform at 100 Hz is shown in Fig. 9 (dotted/black), at the minimum detectable level of 100  $\mu V_{pp}$ . Referring to Fig. 8(c), the implanted antenna is placed under a 2 mm-thick layer of pig skin. The permittivity and loss tangent of the pig skin are measured using the Agilent 85070E Dielectric Probe Kit and further compared vs. the theoretical skin properties [21] shown in Fig. 10. Results in this case show that neural signals as low as 200  $\mu V_{pp}$  can be retrieved for an electrode impedance of 33 k $\Omega$ . An example demodulated waveform at 100 Hz is shown in Fig. 9 (solid/blue) at the minimum detectable level of 200  $\mu V_{pp}$ . This slight degradation in performance is expected given the losses associated with biological tissues. Indeed, Fig. 11 compares the transmission coefficient between the two antennas in free space and with pig skin used as a separation medium. As seen, the transmission coefficient degrades by  $\sim 3$  dB at 2.4 GHz and by  $\sim 8$  dB at 4.8 GHz. As mentioned in Section III.A, higher signal levels result in less noisy waveforms, while smaller electrode impedances result in improved sensitivity. For comparison, and assuming the same electrode impedance of 33 k $\Omega$ , the sensitivity of the neurosensing system in [3] is 25 times lower. Specific Absorption Rate (SAR) simulations are also performed for the

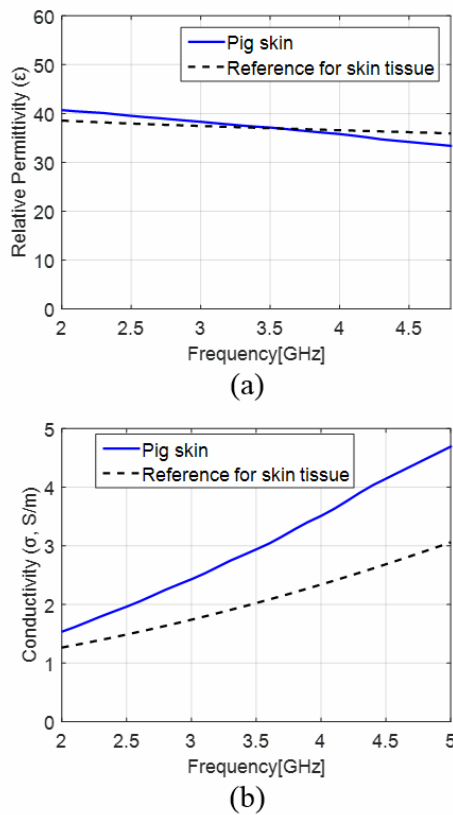


Fig. 10. a) Measured permittivity, and (b) measured conductivity of pig skin versus the reference skin properties reported in [21].

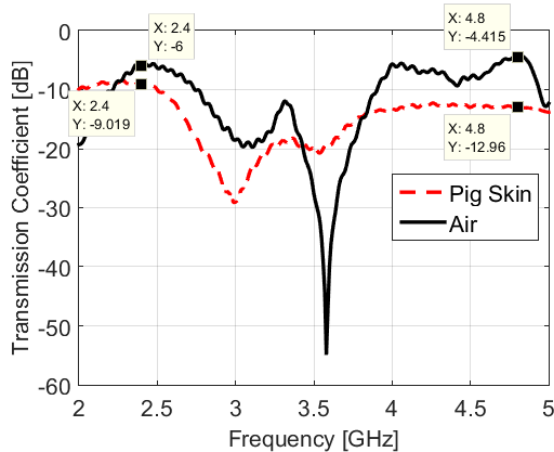


Fig. 11. Measured transmission coefficient ( $S_{21}$ ) of the implanted and interrogator antenna system (a) through air, and (b) through pig skin.

10-cm-radius spherical head model of [3]. Results indicate that SAR averaged over 1g of tissue equals 0.862 W/kg (at 10 dBm power). This value conforms to the strictest FCC requirements of  $SAR_{1g} < 1.6$  W/kg for uncontrolled environment exposure [22].

### C. DC Offset Tolerance

To verify the DC offset tolerance of the implant, the measurement setup of Fig. 8(a) is adopted. In this case, the

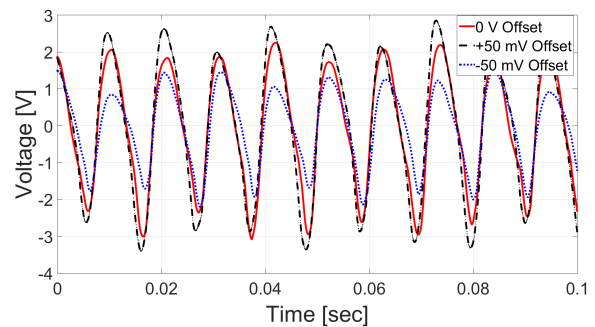


Fig. 12. Demodulated waveform of a  $100 \mu V_{pp}$  and 100 Hz signal subject to: (a) 0 V offset, (b) +50 mV offset, and (c) -50 mV offset in series with a  $33 k\Omega$  resistor

function generator this time provides the emulated neuropotentials as well as an unwanted DC offset voltage. Referring to Fig. 12, demodulated waveforms are presented for a  $100 \mu V_{pp}$  and 100 Hz neural signal subject to: 0 V (solid/red), +50 mV (dashed/black) and -50 mV (dotted/blue) DC offset.

As seen, the proposed implant can tolerate even the most extreme  $\pm 50$  mV DC offset at the minimum detectable level of  $100 \mu V_{pp}$ .

## IV. CONCLUSION

In this work, we proposed a wireless and batteryless brain implant that is matched to the high impedance of recording electrodes as well as resistant to DC offset. Experimental results show that neuropotential detection sensitivity is improved by 25 times vs. the state-of-the-art at an example electrode impedance of  $33 k\Omega$ . Notably, impedance measurements of macroelectrodes using 3-lead electrode impedance spectroscopy indicate that this resistance covers the range anticipated in clinical settings. To date, signals as small as  $100 \mu V_{pp}$  (in free space) and  $200 \mu V_{pp}$  (*in-vitro*, using pig skin) can be captured at a worst-case scenario of  $33 k\Omega$  electrode impedance. This implies that the system can monitor all neural spikes and most of the local field potentials (LFPs) in real-world settings, viz. at high impedances. By contrast, previous wireless and batteryless implants neglected this high impedance and rather matched the implants to a  $50 \Omega$  function generator that emulated brain activity. As such, the proposed approach is transformational for fully-passive and wireless neuropotential acquisition in clinical settings. Future work will focus on: a) implant miniaturization using high-permittivity substrates and stacking approaches (antenna stacked upon the circuit), and b) *in-vivo* testing in animals.

## ACKNOWLEDGMENT

The authors would like to thank Prof. Liang Guo in The Ohio State University ECE department for electrode impedance modeling and Prof. Vibhor Krishna in The Ohio State University Wexner Center for providing the clinical electrode.

## REFERENCES

- [1] C. W. Lee, A. Kiourti, J. Chae, and J. L. Volakis, "A high-sensitivity fully passive neurosensing system for wireless brain signal monitoring," *IEEE Transactions on Microwave Theory and Techniques*, vol. 63, no. 6, pp. 2060–2068, 2015.
- [2] A. Kiourti, C. W. Lee, J. Chae, and J. L. Volakis, "A wireless fully passive neural recording device for unobtrusive neuropotential monitoring," *IEEE Trans. Biomed. Engineering*, vol. 63, no. 1, pp. 131–137, 2016.
- [3] C. W. Lee, A. Kiourti, and J. L. Volakis, "Miniaturized fully passive brain implant for wireless neuropotential acquisition," *IEEE Antennas and Wireless Propagation Letters*, vol. 16, pp. 645–648, 2017.
- [4] W. Chen, C. W. L. Lee, A. Kiourti, and J. L. Volakis, "A multi-channel passive brain implant for wireless neuropotential monitoring," *IEEE Journal of Electromagnetics, RF and Microwaves in Medicine and Biology*, vol. 2, no. 4, pp. 262–269, Dec 2018.
- [5] H. N. Schwerdt, W. Xu, S. Shekhar, A. Abbaspour-Tamijani, B. C. Towe, F. A. Miranda, and J. Chae, "A fully passive wireless microsystem for recording of neuropotentials using rf backscattering methods," *Journal of Microelectromechanical Systems*, vol. 20, no. 5, pp. 1119–1130, 2011.
- [6] H. N. Schwerdt, F. A. Miranda, and J. Chae, "Wireless fully passive multichannel recording of neuropotentials using photo-activated rf backscattering methods," *IEEE Transactions on Microwave Theory and Techniques*, vol. 63, no. 9, pp. 2965–2970, 2015.
- [7] G. Schalk and E. C. Leuthardt, "Brain-computer interfaces using electrocorticographic signals," *IEEE Reviews in Biomedical Engineering*, vol. 4, pp. 140–154, 2011.
- [8] K. D. Wise, A. M. Sodagar, Y. Yao, M. N. Gulari, G. E. Perlin, and K. Najafi, "Microelectrodes, microelectronics, and implantable neural microsystems," *Proceedings of the IEEE*, vol. 96, no. 7, pp. 1184–1202, July 2008.
- [9] R. R. Harrison, "The design of integrated circuits to observe brain activity," *Proceedings of the IEEE*, vol. 96, no. 7, pp. 1203–1216, 2008.
- [10] R. Muller, H.-P. Le, W. Li, P. Ledochowitsch, S. Gambini, T. Bjorninen, A. Koralek, J. M. Carmena, M. M. Maharbiz, E. Alon *et al.*, "A minimally invasive 64-channel wireless  $\mu$ ecog implant," *IEEE Journal of Solid-State Circuits*, vol. 50, no. 1, pp. 344–359, 2015.
- [11] H. Ando, K. Takizawa, T. Yoshida, K. Matsushita, M. Hirata, and T. Suzuki, "Wireless multichannel neural recording with a 128-mbps uwb transmitter for an implantable brain-machine interfaces," *IEEE transactions on biomedical circuits and systems*, vol. 10, no. 6, pp. 1068–1078, 2016.
- [12] S. Kim, P. Tathireddy, R. A. Normann, and F. Solzbacher, "Thermal impact of an active 3-d microelectrode array implanted in the brain," *IEEE Transactions on Neural Systems and Rehabilitation Engineering*, vol. 15, no. 4, pp. 493–501, Dec 2007.
- [13] E. Bharucha, H. Seprehian, and B. Gosselin, "A survey of neural front end amplifiers and their requirements toward practical neural interfaces," 2014.
- [14] L. A. Geddes, "Historical evolution of circuit models for the electrode-electrolyte interface," *Annals of Biomedical Engineering*, vol. 25, no. 1, p. 1, Jan 1997. [Online]. Available: <https://doi.org/10.1007/BF02738534>
- [15] W. Franks, I. Schenker, P. Schmutz, and A. Hierlemann, "Impedance characterization and modeling of electrodes for biomedical applications," *IEEE Transactions on Biomedical Engineering*, vol. 52, no. 7, pp. 1295–1302, July 2005.
- [16] M. J. Nelson, P. Pouget, E. A. Nilsen, C. D. Patten, and J. D. Schall, "Review of signal distortion through metal microelectrode recording circuits and filters," *Journal of neuroscience methods*, vol. 169 1, pp. 141–57, 2008.
- [17] FHC electrode description. [Online]. Available: <https://www.fh-co.com/>
- [18] A. Bagheri, M. T. Salam, J. L. P. Velazquez, and R. Genov, "Low-frequency noise and offset rejection in dc-coupled neural amplifiers: A review and digitally-assisted design tutorial," *IEEE Transactions on Biomedical Circuits and Systems*, vol. 11, no. 1, pp. 161–176, Feb 2017.
- [19] R. R. Harrison, "A low-power, low-noise cmos amplifier for neural recording applications," in *2002 IEEE International Symposium on Circuits and Systems. Proceedings (Cat. No.02CH37353)*, vol. 5, May 2002, pp. V–V.
- [20] J. Ruiz-Amaya, A. Rodriguez-Perez, and M. Delgado-Restituto, "A low noise amplifier for neural spike recording interfaces," *Sensors*, vol. 15, pp. 25 313–25 335, 09 2015.
- [21] S. Gabriel, R. Lau, and C. Gabriel, "The dielectric properties of biological tissues: Ii. measurements in the frequency range 10 hz to 20 ghz," *Physics in medicine & biology*, vol. 41, no. 11, p. 2251, 1996.
- [22] U. F. C. Commission *et al.*, "Report and order fcc 96–326," 1996.



**Wei-Chuan Chen** (S'17) received the B.S. degree in electrical engineering from the National Taiwan University, Taipei, Taiwan in 2014. He is currently working toward the Ph.D. degree at The Ohio State University, Columbus OH, USA from 2015.

His research interests include antenna design, computational electromagnetic, RF/microwave circuit and its applications in medical.



**Katrina Guido** received a B.S. degree in physics from Stevens Institute of Technology, Hoboken, NJ in 2018. She is currently working toward a doctorate in electrical engineering at The Ohio State University, Columbus, OH.

Her research interests include medical sensing, antennas for medical applications, and bioelectromagnetics.



**Asimina Kiourti** (S'10–M'14) received the Diploma degree in electrical and computer engineering from the University of Patras, Patras, Greece, in 2008, the M.Sc. degree in technologies for broadband communications from University College London, London, U.K., in 2009, and the Ph.D. degree in electrical and computer engineering from the National Technical University of Athens, Athens, Greece, in 2013.

Dr. Kiourti is currently an Assistant Professor of Electrical and Computer Engineering at The Ohio State University and the ElectroScience Laboratory, Columbus, OH, USA. From 2013 to 2016 she served as a Post-Doctoral Researcher and then a Senior Research Associate at the ElectroScience Laboratory. During her career, she has (co-)authored over 35 journal papers, 80 conference papers, and 7 book chapters. Her research interests include wearable and implantable sensors, antennas and electromagnetics for body area applications, and flexible textile-based electronics.

Dr. Kiourti has received several awards and scholarships, including the IEEE Engineering in Medicine and Biology Society (EMB-S) Young Investigator Award for 2014, the IEEE Microwave Theory and Techniques Society (MTTS) Graduate Fellowship for Medical Applications for 2012, and the IEEE Antennas and Propagation Society (AP-S) Doctoral Research Award for 2011. She is currently serving as an Associate Editor for the IEEE Transactions on Antennas and Propagation.